Scientia Iranica A (2019) 26(3), 1169–1181

Sharif University of Technology
Scientia Iranica
Transactions A: Civil Engineering
http://scientiairanica.sharif.edu

An analytical approach to the estimation of optimum river channel dimensions

M. Mahmoudi, M.R. Majdzadeh Tabatabai*, and S. Mousavi Nadoushani

Faculty of Civil, Water and Environmental Engineering, Shahid Beheshti University, Tehran, P.O. Box 16765/1719, Iran.

Received 23 January 2017; received in revised form 6 August 2017; accepted 19 May 2018

KEYWORDS
Extremal hypotheses;
Bank vegetation;
Analytical model.

Abstract. Extremal hypotheses without bank stability constraint typically over-predict and under-predict channel width in large rivers and natural streams, respectively. In general, results obtained from unconstrained extremal hypotheses show inappropriate agreement between predicted and observed dimensions of the rivers. One of the important factors in disparity of the data may be lack of appropriate relationships to assess bank vegetation of the rivers. For this reason, a modified analytical model was developed to reduce the effect of bias by considering bank stability and vegetation. The model took into account channel shape factor, a wide range of bed load equations in the form of excess shear stress, and vegetation quantification, which made it able to predict optimal channel geometry dimensions. Finally, the developed model was calibrated using the field data of the United Kingdom and Iran. In addition to indicating the effect of bank stability and vegetation on estimation of the geometric characteristics of the channel, the obtained results confirmed the efficiency of the constrained model in comparison with the unconstrained model. This study also provides support for the use of the concepts of maximum sediment transporting capacity and minimum stream power for understanding the operation of alluvial rivers.

1. Introduction

In the advent of the new millennium, a great deal of advancement in engineering science has been achieved. However, to the problem of alluvial river response to natural and man induced environmental changes, a simple, reasonable, and understanding solution is still being looked for. In general, there are two principal approaches of analytical and empirical to the determination of stable channel geometry in alluvial rivers of which the application could have advantages and disadvantages [1]. Among analytical models, in the last decades, extremal hypotheses have been used as objective functions to estimate optimum channel dimensions. By means of this type of models, sediment transport and flow resistance equations are applied together with a third equation to predict stable channel dimensions. This equation plays the role of an objective function for optimization and is expressed in terms of stream power, energy dissipation rate, sediment transport, etc. [2]. In the early 1960s, researchers like Leopold and Langbein [3] applied minimum variance theory to the design of stable channel dimensions. Pickup [4] and Kirkby [5] suggested Maximum Sediment Transporting Capacity (MSTC). Yang [6] proposed Minimum Energy Dissipation Rate (MEDR) as a general rule in hydraulics. Although MEDR hypothesis made remarkable progresses in the determination of velocity and sediment concentration, Yang et al. [7]

*. *Corresponding author. Tel.: +98 21 7393-2440; Fax: +98 21 7700-6660*
E-mail addresses: mahsa_mahmoodi_69@yahoo.com (M. Mahmoudi); m_majdzadeh@sbu.ac.ir (M.R. Majdzadeh Tabatabai); sa_mousavi@sbu.ac.ir (S. Mousavi Nadoushani)

doi: 10.24200/sci.2018.20552

indicated that MEDR hypothesis would result in a width to depth ratio of 2, which is hardly encountered in natural rivers. Subsequently, Song and Yang [8] suggested Minimum Unit Stream Power hypothesis (MUSP) on the basis of which a self-formed stable channel might adjust its cross shape and dimensions in such a way that transport of water and sediment could take place at optimum condition. Huang and Nanson [9] also emphasized that the stable condition of adjustable alluvial rivers was equivalent to the condition at which the maximum sediment load was transported. Due to insufficient basic flow relationships (i.e., continuity, resistance, and sediment) for expressing the equilibrium state, they recommended the application of extremal hypothesis. In their opinion, the higher number of unknowns than the number of equations might be resolved by defining channel shape factor (width/depth). They calculated optimum shape factor by assuming rectangular cross section and solving basic flow equations together with extremal hypothesis, simultaneously. They derived hydraulic geometry relationships analytically similar to others. They also defined Maximum Flow Efficiency (MFE) as the flow at which maximum sediment transporting capacity occurred per available stream power unit.

Later on, Eaton and Millar [10] applied MTC hypothesis with bank stability constraint by considering trapezoidal shape for the cross section under Parker's bed load [11] and Manning's flow resistance equations [12]. They showed that channel geometry depended upon bank material and vegetation.

Investigations state that results obtained by applying extremal hypotheses without bank stability constraint (unconstrained model) show a relative disagreement between observed and predicted channel geometries, particularly in large rivers [13]. For this reason, an analytical model is developed to accomplish an unconstrained model in which effect of bank stability and vegetation is considered to estimate channel dimensions of gravel bed rivers. The model is able to predict optimum channel dimensions under static and dynamic equilibrium by considering shape factor in trapezoidal form together with a wide range of flow resistance and sediment transport equations as a function of excess bed shear stress. According to Knighton [14] and Lane [15], when the ratio of river design discharge to the threshold discharge of the sediment motion is about 1 or smaller, or, in other words, the entrainment of sediments from the river bed and banks is zero (flow can carry sediments, but cannot erode the river boundaries), the river is considered in the static stability condition. However, when the ratio is larger than 1 (sediments are transported from bed and banks, but the erosion and sedimentation rates are almost the same), the river is considered in the dynamic stability condition. In general, this model is meant to follow Huang and Nanson [9] and couples up with Eaton and Millar [10]. The aim of the presented model in this study is to design dimensions of a stable section carrying a dominant discharge equal to the discharge in the actual river section with the same parameters, such as the Manning's roughness coefficient, longitudinal slope, bank vegetation, and bed and bank materials. In other words, the model is meant to be a practical tool for river restoration and engineering applications, e.g., river dredging. Attempts have been made to design a section that would:

1. Have stable characteristics;
2. Pass a discharge equal to the river dominant discharge.

2. Material and methods

Selection of dependent and independent variables is one of the most important problems suggested in analytical models. The suggested model may be proper to both constant and variable slopes. For constant slope, the model input data are dominant discharge, longitudinal slope, bed and bank material size, friction angle of bank material, and roughness coefficient, while in the case of variable slope, slope is replaced by sediment transport rate in input data to work out the optimum slope. River cross section is considered trapezoidal with constant side slope of 1 (horizontal): z (vertical).

In Figure 1, P_{bed}, P_{bank}, W, D, z, and ϕ' are bed perimeter, bank perimeter, channel surface width, maximum channel depth, bank slope (θ is bank angle), and bank friction angle, respectively. According to Eaton and Millar, and Lane, in natural rivers, the angle between banks of the channel and floodplain surface can be considered as ϕ' [10,15]. Bed and banks may be easily distinguishable by Parker's definition, followed by proceeding from the floodplain margins to the center of the river channel and getting to the first point with the depth of $0.99D$ max, to determine the river bank area [17].

2.1. Model assumptions

- Flow is steady and uniform;
- The model is applicable to straight reach of the river, through which sediment is mainly transported as bedload;

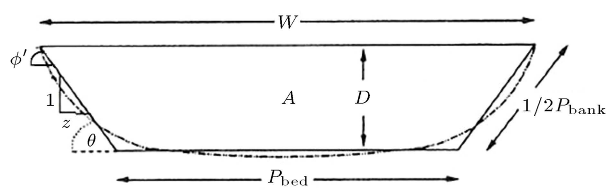

Figure 1. River cross section [16].

- Bed and bank are mainly composed of coarse grain sized materials; hence, resistance due to form roughness is negligible;
- River cross section is in trapezoidal form;
- Stability is achieved by satisfying extremal hypotheses;
- Dominant discharge is considered to be estimated by bankfull discharge.

2.2. Governing flow equations

There are six equations to develop channel geometry, namely continuity, resistance, sediment transport, mean bank shear stress, mean bed shear stress, and bank stability, whereas seven dependent variables are available, namely bed perimeter (P_{bed}), maximum channel depth (D), longitudinal slope (S) (in constant slope state) or bed load discharge (Q_s) (in variable slope state), mean velocity (V), mean bank shear stress ($\bar{\tau}_{\text{bank}}$), mean bed shear stress ($\bar{\tau}_{\text{bed}}$), and bank angle (θ). To estimate these variables, it is required to have seven equations as well. This made the authors use extremal hypothesis as the seventh equation. The equations are defined as follows:

Flow continuity to be maintained in alluvial channels is:

$$Q = A \times V, \tag{1}$$

in which A, V, and Q are cross sectional area, average flow velocity, and dominant or bankfull flow discharge, respectively.

In the model, a generalized form of flow resistance based on Huang and Nanson [9] with some modifications may be expressed as:

$$V = c_r R^x S^y D^{\alpha}, \tag{2}$$

in which c_r is a coefficient determined by sediment size; x, y, and α are functions of channel bed forms or flow regimes; and R is hydraulic radius. Many resistance equations, such as Manning [12], Lacey [18], Brownlie [19], etc., may be same as the above.

To avoid a particular equation of bed load in the model, a general form of the bed load equation in the form of excess bed shear stress was initially suggested by Huang and Nanson [9]. Although there are bed load equations with no sediment threshold of motion [20], hydraulic engineers emphasize the determination of sediment threshold of motion. As this is the state at which sediment particles are in equilibrium, its formulation will help in solving problems such as non-erodible stable channel design, riprap size design to protect bed and banks of the channels, and calculation of sediment transport in rivers [21].

$$q_s = c_s \bar{\tau}_{\text{bed}}^m \left(\bar{\tau}_{\text{bed}} - \tau_c\right)^j, \tag{3}$$

where q_s, c_s, $\bar{\tau}_{\text{bed}}$, and τ_c are bed load discharge per unit channel width, a constant relating to sediment characteristics, mean bed shear stress, and critical shear stress for the incipient motion of sediments, respectively. Exponents m and j vary widely, as shown in many bed load transport models. Huang and Nanson [9] indicated that the above equation could easily be in the form of Meyer-Peter and Muller [22], Du Boys [23], Parker [24], etc.

In this paper, Flintham and Carling [25] relations for trapezoidal section, which were initially derived by Knight [26] and Knight et al. [27], are used to estimate boundary shear stress distribution. The proportion of the shear force acting on the bank (SF_{bank}) and the mean bank and bed shear stress values ($\bar{\tau}_{\text{bank}}$ and $\bar{\tau}_{\text{bed}}$, respectively) are estimated using the following equations:

$$\log \%SF_{\text{bank}} = -1.4026 \log\left(\frac{P_{\text{bed}}}{P_{\text{bank}}} + 1.5\right) + 2.247, \tag{4}$$

$$\frac{\bar{\tau}_{\text{bank}}}{\gamma DS} = 0.01\%SF_{\text{bank}} \left[\frac{(W + P_{\text{bed}})\sin\theta}{4D}\right], \tag{5}$$

$$\frac{\bar{\tau}_{\text{bed}}}{\gamma DS} = (1 - 0.01\%SF_{\text{bank}}) \left[\frac{W}{2P_{\text{bed}}} + 0.5\right], \tag{6}$$

where γ is unit weight of water. The rest of the parameters are same as before. It is necessary to notice that in trapezoidal channel, $P_{\text{bank}} = 2D\sqrt{1 + z^2}$.

The stability of the bank is assessed by comparing the value of $\bar{\tau}_{\text{bank}}$ calculated from Eq. (5) with a modified USBR bank stability criterion (after Eaton and Millar [10]), based on the bank sediment caliber ($D_{50\text{bank}}$) and bank friction angle (ϕ'):

$$\tau_{cb}^* = \bar{\tau}_{\text{bank}} / ((\gamma_s - \gamma)\, D_{50\text{bank}}) = c \tan\phi' \sqrt{1 - (\sin^2\theta / \sin^2\phi')}. \tag{7}$$

The coefficient c is dependent upon the properties of the unconsolidated, non-cohesive sediment, where bank strength is unmodified by bank vegetation. The coefficient is defined as [28]:

$$c = \tau_c^* / \tan\phi, \tag{8}$$

in which τ_c^* is the critical dimensionless shear stress for bed material of the same caliber and ϕ is the angle of repose.

The value of ϕ varies with grain size and shape [28], ranging from a minimum of about 25° for fine sand to about 40° for sub-rounded gravel. Setting $\tau_c^* \approx 0.04$, c will vary between about 0.086-0.048. In this paper, we use $c = 0.048$ for natural gravel rivers. The value of ϕ' ranges from a lower bound of $\phi' = \phi$, where the where the bank sediment is unaffected by bank vegetation or interstitial cohesive sediment, up to a maximum value approaching 90°, which corresponds to a non-erodible bank [10]. Here, MSTC and MSP hypotheses are combined as the seventh equation proper to an alluvial river to adjust its slope and geometry for maximizing sediment transport.

2.3. Theory

As it was mentioned, the model is meant to follow Huang and Nanson [9] and couples up with Eaton and Millar [10].

First, a non-dimensional channel shape factor ζ is defined as:

$$\zeta = P_{\text{bed}}/D, \tag{9}$$

by which trapezoidal cross section geometric parameters are expressed as:

$$A = D^2(\zeta + z), \tag{10}$$

$$P = P_{\text{bed}} + P_{\text{bank}} = D\left(\zeta + 2\sqrt{1+z^2}\right), \tag{11}$$

$$R = A/P = \frac{(\zeta+z)}{\left(\zeta + 2\sqrt{1+z^2}\right)}D, \tag{12}$$

$$W = P_{\text{bed}} + 2zD = D(\zeta + 2z). \tag{13}$$

To determine the relationship of depth with ζ, Q, z, S, and c_r, it is sufficient to substitute Q/A from Eq. (1) for the velocity in Eq. (2) and incorporate the result into Eqs. (10) and (11):

$$D = \frac{\left(\zeta + 2\sqrt{1+z^2}\right)^{x/(x+2+\alpha)}}{(\zeta+z)^{(x+1)/(x+2+\alpha)}}\frac{(Q/c_r)^{1/(x+2+\alpha)}}{S^{y/(x+2+\alpha)}}. \tag{14}$$

By incorporating Eq. (14) with Eqs. (5), (6), and (9)-(12), the relationships are derived to estimate P_{bed}, V, $\bar{\tau}_{\text{bed}}$, and $\bar{\tau}_{\text{bank}}$ in terms of ζ, Q, z, S, and c_r:

$$P_{\text{bed}}(=\zeta D) = \frac{\zeta\left(\zeta + 2\sqrt{1+z^2}\right)^{x/(x+2+\alpha)}}{(\zeta+z)^{(x+1)/(x+2+\alpha)}} \frac{(Q/c_r)^{1/(x+2+\alpha)}}{S^{y/(x+2+\alpha)}}, \tag{15}$$

$$V(=Q/A) = \frac{\left(S^{2y}Q^{(x+\alpha)}c_r^2\right)^{1/(x+2+\alpha)}(\zeta+z)^{(x-\alpha)/(x+2+\alpha)}}{\left(\zeta+2\sqrt{1+z^2}\right)^{(2x)/(x+2+\alpha)}}, \tag{16}$$

$$\bar{\tau}_{\text{bed}} = \gamma DS(1 - 0.01\%SF_{\text{bank}})\left(\frac{\zeta+z}{\zeta}\right), \tag{17}$$

$$\bar{\tau}_{\text{bank}} = \gamma DS \times 0.01\%SF_{\text{bank}}\left[\frac{(\zeta+z)\sin\theta}{2}\right]. \tag{18}$$

Value of D can be replaced in Eqs. (17) and (18) from Eq. (14). $\%SF_{\text{bank}}$ can be estimated in terms of ζ and z as:

$$\%SF_{\text{bank}} = 10^{2.247}\left(\frac{\zeta}{2\sqrt{1+z^2}} + 1.5\right)^{-1.4026}. \tag{19}$$

Huang and Nanson [9] suggested that channel slope, S, could be regarded as a function of channel shape factor ζ, $S = S(\zeta)$; therefore, $P_{\text{bed}} = P_{\text{bed}}(\zeta, S(\zeta))$, $D = D(\zeta, S(\zeta))$, and $\bar{\tau}_{\text{bed}} = \bar{\tau}_{\text{bed}}(\zeta, S(\zeta))$; leading to:

$$\frac{dP_{\text{bed}}}{d\zeta} = \frac{\partial P_{\text{bed}}}{\partial \zeta} + \frac{\partial P_{\text{bed}}}{\partial S}\frac{dS}{d\zeta}, \tag{20a}$$

$$\frac{d\bar{\tau}_{\text{bed}}}{d\zeta} = \frac{\partial \bar{\tau}_{\text{bed}}}{\partial \zeta} + \frac{\partial \bar{\tau}_{\text{bed}}}{\partial S}\frac{dS}{d\zeta}, \tag{20b}$$

where Eqs. (15) and (17) give:

$$\frac{\partial P_{\text{bed}}}{\partial \zeta} = \left[\frac{(1+x+\alpha)\zeta + 2(1+\alpha)\sqrt{1+z^2}}{\left(\zeta+2\sqrt{1+z^2}\right)(\zeta+z)(2+x+\alpha)} + \frac{(2+2x+\alpha)z + \frac{(4+2x+2\alpha)z\sqrt{1+z^2}}{\zeta}}{\left(\zeta+2\sqrt{1+z^2}\right)(\zeta+z)(2+x+\alpha)}\right]P_{\text{bed}},$$

$$\frac{\partial P_{\text{bed}}}{\partial S} = \frac{-y}{(2+x+\alpha)S}P_{\text{bed}}, \tag{21a}$$

Eq. (21b) is shown in Box I.

To have an in-depth understanding of the variations of bed width, depth, and mean bed shear stress with shape factor, it is required to determine $S = S(\zeta)$. The following section shows that obtaining the explicit relationship of $S = S(\zeta)$ is still impossible with selection of a bed load equation due to the lack of an extra flow equation.

Letting Q_s be sediment discharge on total channel width and because $Q_s = P_{\text{bed}}q_s$, $P_{\text{bed}} = P_{\text{bed}}(\zeta, S(\zeta))$, $\bar{\tau}_{\text{bed}} = \bar{\tau}_{\text{bed}}(\zeta, S(\zeta))$, and thus $Q_s = Q_s(\zeta, S(\zeta))$, the following relationship is maintained:

$$\frac{dQ_s}{d\zeta} = \frac{\partial Q_s}{\partial \zeta} + \frac{\partial Q_s}{\partial S}\frac{dS}{d\zeta}, \tag{22}$$

where the selected bed load transport relationships of $q_s = c_s\bar{\tau}_{\text{bed}}^m(\bar{\tau}_{\text{bed}} - \tau_c)^j$ and $Q_s = P_{\text{bed}}q_s$ give:

$$\frac{\partial Q_s}{\partial \zeta} = \frac{\partial Q_s}{\partial \tau_0}\frac{\partial \bar{\tau}_{\text{bed}}}{\partial \zeta} + \frac{\partial Q_s}{\partial P_{\text{bed}}}\frac{\partial P_{\text{bed}}}{\partial \zeta} = Q_s\left[\left(\frac{m}{\bar{\tau}_{\text{bed}}} + \frac{j}{(\bar{\tau}_{\text{bed}} - \tau_c)}\right)\frac{\partial \bar{\tau}_{\text{bed}}}{\partial \zeta} + \frac{1}{P_{\text{bed}}}\frac{\partial P_{\text{bed}}}{\partial \zeta}\right], \tag{23a}$$

$$\frac{\partial \bar{\tau}_{\mathrm{bed}}}{\partial \zeta} = \left[\frac{-\zeta - 2(1+x)\sqrt{1+z^2} - (2+\alpha)z - 2(2+x+\alpha)\dfrac{z\sqrt{1+z^2}}{\zeta}}{\left(\zeta + 2\sqrt{1+z^2}\right)(\zeta+z)(2+x+\alpha)} \right.$$

$$\left. + \frac{0.01 \times 10^{2.247} \times 1.4026(1-0.01\%SF_{\mathrm{bank}})^{-1}}{2\sqrt{1+z^2}\left(\frac{\zeta}{2\sqrt{1+z^2}} + 1.5\right)^{2.4026}} \right] \bar{\tau}_{\mathrm{bed}},$$

$$\frac{\partial \bar{\tau}_{\mathrm{bed}}}{\partial S} = \frac{(2+x+\alpha-y)}{(2+x+\alpha)S}\bar{\tau}_{\mathrm{bed}}. \tag{21b}$$

Box I

$$\frac{\partial Q_s}{\partial S} = \frac{\partial Q_s}{\partial \tau_0}\frac{\partial \bar{\tau}_{\mathrm{bed}}}{\partial S} + \frac{\partial Q_s}{\partial P_{\mathrm{bed}}}\frac{\partial P_{\mathrm{bed}}}{\partial S}$$

$$= Q_s \left[\left(\frac{m}{\bar{\tau}_{\mathrm{bed}}} + \frac{j}{(\bar{\tau}_{\mathrm{bed}} - \tau_c)} \right) \frac{\partial \bar{\tau}_{\mathrm{bed}}}{\partial S} + \frac{1}{P_{\mathrm{bed}}}\frac{\partial P_{\mathrm{bed}}}{\partial S} \right]. \tag{23b}$$

Incorporating the expressions $\frac{\partial P_{\mathrm{bed}}}{\partial \zeta}$, $\frac{\partial P_{\mathrm{bed}}}{\partial S}$, $\frac{\partial \bar{\tau}_{\mathrm{bed}}}{\partial \zeta}$, and $\frac{\partial \bar{\tau}_{\mathrm{bed}}}{\partial S}$ in Eqs. (21a), (21b) into Eq. (23a), (23b) produces Eq. (24a) and (24b) as shown in Box II.

Now, to determine optimum cross section characteristics, Q_s is differentiated with respect to ζ and made equal to zero; consequently, from Eq. (22), it results that:

$$\frac{dS}{d\zeta} = -\frac{\partial Q_s/\partial \zeta}{\partial Q_s/\partial S}. \tag{25}$$

From Eqs. (24a), (24b), and (25), it is clear that variations of $dS/d\zeta$ depend on variations of $\bar{\tau}_{\mathrm{bed}}/\tau_c$ and ζ. For given values of the ratio of $\bar{\tau}_{\mathrm{bed}}/\tau_c$, $dS/d\zeta$ varies from negative to positive values by increase in the value of ζ. This means that there is an upward concavity in $S-\zeta$ plot and S reaches its lowest value when it intersects with the horizontal axis.

2.4. Optimum dimensions of channel cross section ($Q_s = Q_{s\,\max}$)

Now, with regards to Eq. (25), to minimize the slope of

$$\frac{\partial Q_S}{\partial \zeta} = \left[\frac{(x+1+\alpha)\zeta + 2(1+\alpha)\sqrt{1+z^2} + (2+2x+\alpha)z + \frac{(4+2x+2\alpha)z\sqrt{1+z^2}}{\zeta}}{\left(\zeta+2\sqrt{1+z^2}\right)(\zeta+z)(2+x+\alpha)} \right.$$

$$\left. -K\frac{(m+j)\bar{\tau}_{\mathrm{bed}} - m\tau_c}{\left(\zeta+2\sqrt{1+z^2}\right)(\zeta+z)(2+x+\alpha)(\bar{\tau}_{\mathrm{bed}}-\tau_c)} \right] Q_S, \tag{24a}$$

where:

$$K = -\left\{ \frac{2\sqrt{1+z^2}\left(\frac{\zeta}{2\sqrt{1+z^2}}+1.5\right)^{2.4026}\left[-\zeta-(2+\alpha)z-2(1+x)\sqrt{1+z^2}-\frac{2(2+x+\alpha)z\sqrt{1+z^2}}{\zeta}\right]}{2\sqrt{1+z^2}\left(\frac{\zeta}{2\sqrt{1+z^2}}+1.5\right)^{2.4026}} \right.$$

$$\left. + \frac{0.01\times 10^{2.247}\times 1.4026(1-0.01\%SF_{\mathrm{bank}})^{-1}(\zeta+2\sqrt{1+z^2})(\zeta+z)(x+2+\alpha)}{2\sqrt{1+z^2}\left(\frac{\zeta}{2\sqrt{1+z^2}}+1.5\right)^{2.4026}} \right\},$$

$$\frac{\partial Q_S}{\partial S} = \left\{ \frac{[(x+2+\alpha-y)(m+j)-y]\tau_0}{S(2+x+\alpha)(\tau_0-\tau_c)} + \frac{[y-m(x+2+\alpha-y)]\tau_c}{S(2+x+\alpha)(\tau_0-\tau_c)} \right\} Q_S. \tag{24b}$$

Box II

$$\bar{\tau}_{\text{bed}} = \tau_c \frac{(x+1+\alpha)\zeta_m + 2(1+\alpha)\sqrt{1+z^2} + (2+2x+\alpha)z + \frac{(4+2x+2\alpha)z\sqrt{1+z^2}}{\zeta_m} - mK}{(x+1+\alpha)\zeta_m + 2(1+\alpha)\sqrt{1+z^2} + (2+2x+\alpha)z + \frac{(4+2x+2\alpha)z\sqrt{1+z^2}}{\zeta_m} - (m+j)K}. \tag{26}$$

Box III

($dS/d\zeta = 0$), $\partial Q_s/\partial\zeta$ should be equal to zero as shown in Box III, in which K is calculated from Eq. (24a). In the above equation, for given values of Q, S, c_r, and D_{50} (i.e. constant slope), shape factor (ζ) and bank slope (z) are unknowns, therefore, another equation is required. This may be obtained by coupling USBR modified bank stability equation (Eq. (7)) to mean bank shear stress (Eq. (18)).

$$DS \times 0.01\% SF_{\text{bank}} \left[\frac{(\zeta+z)\sin\theta}{2}\right]$$

$$= 0.048(G_s - 1)D_{50\text{bank}} \tan\phi' \sqrt{1 - \frac{\sin^2 heta}{\sin^2\phi'}}, \tag{27}$$

in which D is calculated from Eq. (14). By solving Eqs. (26) and (27) simultaneously, optimum values of shape factor (ζ) and bank slope (z) are computed and, by substituting these values into Eqs. (14) to (17), D_m, $(P_{bed})_m$, V_m, and $(\bar{\tau}_{\text{bed}})_m$ are computed likewise for other parameters. Optimum channel slope may also be computed by applying Eqs. (17) and (26) as shown in Box IV.

By substituting S_m from Eq. (28) into Eqs. (14) and (15), relationships of bed width ($(P_{\text{bed}})_m$) and maximum depth (D_m) are derived (variable slope) which is shown in Box V.

Substituting Eq. (30) into Eq. (13), the relationship of optimum surface width is produced by Eq. (31) as shown in Box VI. Incorporating the expressions $(P_{\text{bed}})_m$ and $(\bar{\tau}_{\text{bed}})_m$ in Eqs. (26) and (29) into:

$$Q_s = P_{\text{bed}} c_s \bar{\tau}_{\text{bed}}^m (\bar{\tau}_{\text{bed}} - \tau_c)^j,$$

$$S_m = \left(\left(\frac{c_r}{Q}\right)\left(\frac{\tau_c}{\gamma}\right)^{(x+2+\alpha)}\right)^{\frac{1}{x+2+\alpha-y}} \frac{((1-0.01\% SF_{\text{bank}})^{-1}\zeta_m)^{(2+x+\alpha)(x+2+\alpha-y)}}{(\zeta_m+z)^{(1+\alpha)/(x+2+\alpha-y)}\left(\zeta_m + 2\sqrt{1+z^2}\right)^{x/(x+2+\alpha-y)}}$$

$$\times\left(\frac{(x+1+\alpha)\zeta_m + 2(1+\alpha)\sqrt{1+z^2} + (2+2x+\alpha)z + \frac{(4+2x+2\alpha)z\sqrt{1+z^2}}{\zeta_m} - mK}{(x+1+\alpha)\zeta_m + 2(1+\alpha)\sqrt{1+z^2} + (2+2x+\alpha)z + \frac{(4+2x+2\alpha)z\sqrt{1+z^2}}{\zeta_m} - (m+j)K}\right)^{\frac{(x+2+\alpha)}{(x+2+\alpha-y)}}. \tag{28}$$

Box IV

$$(P_{\text{bed}})_m = \left(\frac{Q\gamma^y}{c_r\tau_c^y}\right)^{\frac{1}{(x+2+\alpha-y)}} \frac{\left((1-0.01\% SF_{\text{bank}})^y \zeta_m^{x+2+\alpha-2y}\right)^{1/(x+2+\alpha-y)}\left(\zeta_m + 2\sqrt{1+z^2}\right)^{x/(x+2+\alpha-y)}}{(\zeta_m+z)^{(y-x-1)/(x+2+\alpha-y)}}$$

$$\times\left(\frac{(x+1+\alpha)\zeta_m + 2(1+\alpha)\sqrt{1+z^2} + (2+2x+\alpha)z + \frac{(4+2x+2\alpha)z\sqrt{1+z^2}}{\zeta_m} - (m+j)K}{(x+1+\alpha)\zeta_m + 2(1+\alpha)\sqrt{1+z^2} + (2+2x+\alpha)z + \frac{(4+2x+2\alpha)z\sqrt{1+z^2}}{\zeta_m} - mK}\right)^{\frac{y}{(x+2+\alpha-y)}} \tag{29}$$

$$D_m = \left(\frac{Q\gamma^y}{c_r\tau_c^y}\right)^{\frac{1}{(x+2+\alpha-y)}} \frac{\left((1-0.01\% SF_{\text{bank}})^y \zeta_m^{-y}\right)^{1/(x+2+\alpha-y)}\left(\zeta_m + 2\sqrt{1+z^2}\right)^{x/(x+2+\alpha-y)}}{(\zeta_m+z)^{(y-x-1)/(x+2+\alpha-y)}}$$

$$\times\left(\frac{(x+1+\alpha)\zeta_m + 2(1+\alpha)\sqrt{1+z^2} + (2+2x+\alpha)z + \frac{(4+2x+2\alpha)z\sqrt{1+z^2}}{\zeta_m} - (m+j)K}{(x+1+\alpha)\zeta_m + 2(1+\alpha)\sqrt{1+z^2} + (2+2x+\alpha)z + \frac{(4+2x+2\alpha)z\sqrt{1+z^2}}{\zeta_m} - mK}\right)^{\frac{y}{(x+2+\alpha-y)}}. \tag{30}$$

Box V

$$W_m = \left(\frac{Q\gamma^y}{c_r\tau_c^y}\right)^{\frac{1}{(x+2+\alpha-y)}} \frac{\left((1-0.01\%SF_{\text{bank}})^y\zeta_m^{-y}(\zeta_m+2z)^{(x+2+\alpha-y)}\left(\zeta_m+2\sqrt{1+z^2}\right)^x\right)^{1/(x+2+\alpha-y)}}{(\zeta_m+z)^{(y-x-1)/(x+2+\alpha-y)}}$$
$$\times\left(\frac{(x+1+\alpha)\zeta_m+2(1+\alpha)\sqrt{1+z^2}+(2+2x+\alpha)z+\frac{(4+2x+2\alpha)z\sqrt{1+z^2}}{\zeta_m}-(m+j)K}{(x+1+\alpha)\zeta_m+2(1+\alpha)\sqrt{1+z^2}+(2+2x+\alpha)z+\frac{(4+2x+2\alpha)z\sqrt{1+z^2}}{\zeta_m}-mK}\right)^{\frac{y}{(x+2+\alpha-y)}}. \quad (31)$$

Box VI

$$Q_s(=Q_{s\max}) = j^j c_s \gamma^{\frac{y}{(x+2+\alpha-y)}} \tau_c^{m+j-\frac{y}{(x+2+\alpha-y)}} (Q/c_r)^{\frac{1}{(x+2+\alpha-y)}} K^j$$
$$\times\frac{\left((x+1+\alpha)\zeta_m+2(1+\alpha)\sqrt{1+z^2}+(2+2x+\alpha)z+\frac{(4+2x+2\alpha)z\sqrt{1+z^2}}{\zeta_m}-mK\right)^{m-\frac{y}{(x+2+\alpha-y)}}}{\left((x+1+\alpha)\zeta_m+2(1+\alpha)\sqrt{1+z^2}+(2+2x+\alpha)z+\frac{(4+2x+2\alpha)z\sqrt{1+z^2}}{\zeta_m}-(m+j)K\right)^{m+j-\frac{y}{(x+2+\alpha-y)}}}$$
$$\times\left[\frac{(1-0.01\%SF_{\text{bank}})^y\zeta_m^{(x+2+\alpha-2y)}(\zeta_m+2\sqrt{1+z^2})^x}{(\zeta_m+z)^{(-x+y-1)}}\right]^{\frac{1}{(x+2+\alpha-y)}}. \quad (32)$$

Box VII

$Q_{s\max}$ is maintained as shown in Box VII, in which K is calculated from Eq. (24a). As in stable channels, $Q_{s\max} = Q_s$; therefore, for given Q_s, optimum shape factor (ζ) and stable bank slope (z) can be computed by solving Eqs. (27) and (32), simultaneously, for variable slope condition. In fact, in this case, the slope of the river is adjusted in such a way that it can transport inflow of water and sediment. It is noticeable that in $Q_s = P_{\text{bed}}c_s\bar{\tau}_{\text{bed}}^m(\bar{\tau}_{\text{b ed}}-\tau_c)^j$, if $\bar{\tau}_{\text{bed}} < \tau_c$, $\bar{\tau}_{\text{bed}}$ is considered to be equal to τ_c for stable channel design, in which $Q_s = 0$. In other words, channel dimensions are designed for bed sediment threshold of motion, which may be interpreted as static stability of the channel. Under these circumstances, Eq. (26) may be applied as:

$$Kj = 0 \Rightarrow K = 0 \Rightarrow 0.01\times 10^{2.247} \times 1.4026(1-0.01\%SF_{\text{bank}})^{-1}$$
$$\left(\zeta_m+2\sqrt{1+z^2}\right)(\zeta_m+z)(x+2+\alpha)$$
$$=-2\sqrt{1+z^2}\left(\frac{\zeta_m}{2\sqrt{1+z^2}}+1.5\right)^{2.4026}$$
$$\left[-\zeta_m-(2+\alpha)z-2(x+1)\sqrt{1+z^2} - 2(x+2+\alpha)\frac{z\sqrt{1+z^2}}{\zeta_m}\right]. \quad (33)$$

With regards to Eq. (26), if $K = 0$ (i.e., Eq. (33)), $Q_s = 0$, which conforms to the sediment threshold of motion. Likewise, for $\partial\bar{\tau}_{\text{bed}}/\partial\zeta = 0$, from Eq. (21b), Eq. (33) is resulted and bed shear stress reaches its maximum value, which again confirms the sediment threshold. This equation could be applied for static equilibrium in channel, when flow can transport sediment without erosion in the channel [14,15].

3. Results and discussion

3.1. Sensitivity analysis

In this section, effect of modified bank friction angle (ϕ') on river geometry is investigated by applying Manning's roughness [12] and MPM [22] and Parker [24] bed load equations, where other input variables are kept constant (Figure 2). It is noticed that with increase in ϕ', surface width (W) decreases while water depth (D) increases. This could be justified by the fact that as ϕ' increases (i.e., bank vegetation increases), bank resistance also increases and, therefore, bed sediments are more exposed to erosion than the banks are, which may cause channel deepening. This could also be confirmed by velocity reduction in the vicinity of the banks, which leads to the situation in which deposition

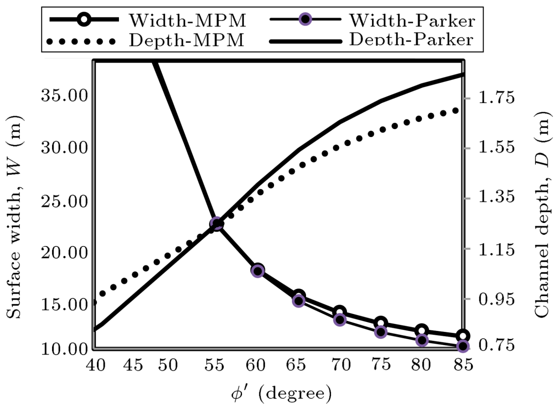

Figure 2. Sensitivity analysis of ϕ' to water surface width and depth.

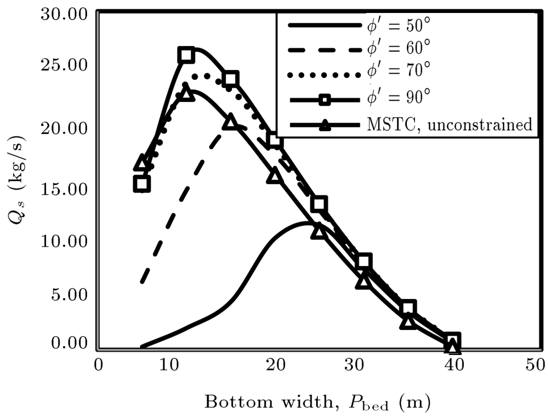

Figure 3. Variations of computed bed load versus bed width for different values of ϕ'.

occurs faster. This figure also indicates that ϕ' could be effective on river geometry in such a way that with its variation from 40° to 60°, the highest variations occur in width and depth, while under its variation from 60° to 90°, variations of width and depth decrease. In general, it is obvious that the above bed load equations have the same function with respect to ϕ'.

Furthermore, sensitivity analysis was carried out by keeping Q, S, D_{50}, and c_s constant for four different values of ϕ' (namely 50°, 60°, 70°, and 90°) to compute variations of bed load transport, using MPM [22] equation, versus bed width (P_{bed}). It is worth mentioning that the above analysis was also conducted for the unconstrained model under two extremal hypotheses of MSTC and MSP (Figure 3). This illustrates that with increase in ϕ', optimum bed width decreases and maximum sediment transport increases.

Sensitivity analysis was also conducted on variations of $D_{50\text{bank}}$ using MPM [22] and Parker [24] equations (Figure 4). It shows that with increase in $D_{50\text{bank}}$, surface width decreases while increasing depth. The results also state that channel geometry is most sensitive to $D_{50\text{bank}}$ with values up to 0.05 m while for $D_{50\text{bank}} > 0.05$ m, no changes are observed

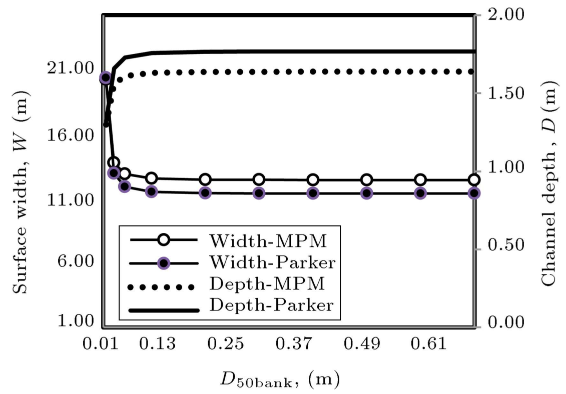

Figure 4. Sensitivity analysis of $D_{50\text{bank}}$ to water surface width and depth.

in the geometry. In other words, in this case, with increase in $D_{50\text{bank}}$, bank stability increases as a result of which channel widening decreases. When bed erosion occurs, the channel may reach the state at which armoring takes place and channel deepening ceases.

3.2. Model calibration

In this study, two case studies are used to calibrate the model as follows:

Case study 1. In this section, Hey and Thorne [29] data set, which was later updated by Darby [30], is used to calibrate the model. The data set consists of 62 river stations with river geometries measured in low flow conditions and characterized as stable single thread with mobile bed; four categories are proposed for bank vegetation density:

- Type 1: represents grassy banks with no trees or bushes;
- Type 2: 1-5% tree/shrub cover;
- Type 3: 5-50% tree/shrub cover;
- Type 4: greater than 50% tree/shrub cover or incised in flood plain.

In this study, $D_{50\text{bank}}$, suggested by Darby [30], does not give good results. However, when $D_{50\text{bank}} = D_{50\text{surface}}$ is considered [10], less discrepancy is observed in the results. This assumption may be in agreement with the case that banks are exposed to erosion and their composition deposits on the river bed.

3.2.1. ϕ' estimation

As it was shown in the section on sensitivity analysis, ϕ' could be the key control parameter in bank stability, the value of which varies with bank vegetation density. It is worth mentioning that these values are not given by Hey and Thorne [29]. Estimation of ϕ' is made for 48 stations in the data and it is done with a particular value of ϕ' for each station; then, the value is

Table 1. Calibrated ϕ' values for different bank vegetation types for 48 stations of Hey and Thorne [29].

Vegetation type	ϕ' (°)		
	Minimum	**Mean**	**Maximum**
1	30.6	43.5	54.2
2	32.6	47.6	59.7
3	35.0	50.0	72.0
4	44.1	64.3	87.0

changed to make the difference between observed and predicted widths approximately ±1% (Table 1). As it is shown, the average ϕ' value for each vegetation type varies with vegetation cover. This confirms that the impact of vegetation cover on channel geometry can be considered by ϕ'.

3.2.2. Comparison of model outputs with field data

In this section, predicted results are plotted against observed data; the predicted results have been obtained by Manning's roughness equation [12] and Parker's bed load equation [24] (Figure 5).

3.3. Effect of bank vegetation

The aim of this section is to investigate the effect of vegetation on estimation of stable width and compare the results of constrained and unconstrained models by considering a combination of MSTC and MSP extremal hypotheses. In order to have deep understanding of the effect of vegetation cover, it is initially considered in two phases of sparse vegetation (Types 1 and 2) and dense vegetation (Types 3 and 4) (Figure 6). The process of analysis is repeated for all types, i.e., 1, 2, 3, and 4 in detail (Table 2). As it is shown in Figure 6(a), channels with observed widths lower than 30 m and sparse bank vegetation are more scattered around the best fit line, while those with dense vegetation are less scattered around the same line. For channel widths greater than 30 m, the discrepancy between the data and the best fit line increases, which brings the behavior of the model into question.

In addition, in Table 2, the observed width values are often greater than the predicted values. $W_{\text{pred}}/W_{\text{obs}}$ in unconstrained model of the combination of MSTC and MSP varies between 0.44-0.75 for bank vegetation Types 1 to 4. In other words, with increase in vegetation type from 1 to 4, bank resistance also increases to meet the assumption of bank inedibility in unconstrained model. Hence, it is expected to have predicted width values much closer to the observed ones in Types 3 and 4 than in Types 1 and 2. With regards to Table 2 and Figure 6, it is obvious that by inserting vegetation cover in the model, in addition to improving the disparity of data around the best fit line, $W_{\text{pred}}/W_{\text{obs}}$ gets closer to 1 for all vegetation types. This confirms the improvement in the accuracy of the model in width prediction by applying bank vegetation.

In the investigation into vegetation impact, many

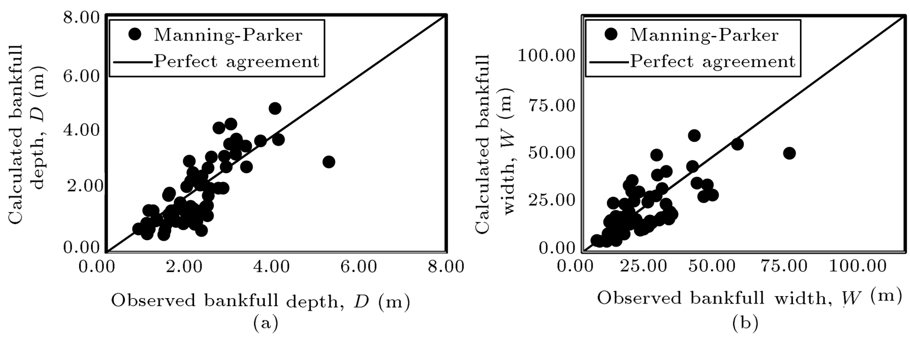

Figure 5. Comparison of calculated versus observed bankfull width and depth.

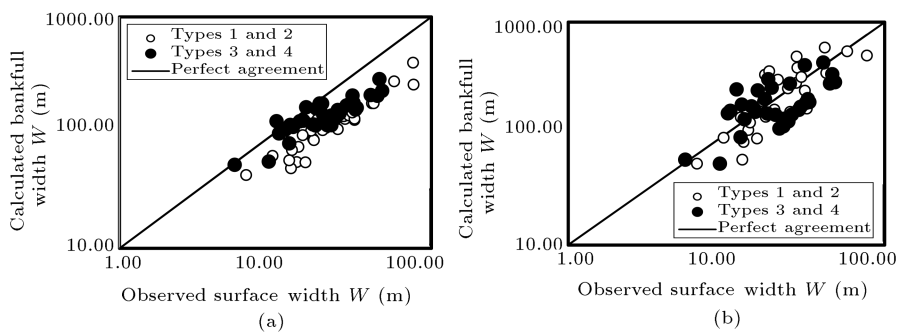

Figure 6. Predicted widths using Parker's equation [24] against the observed widths for gravel bed channels by (a) Unconstrained model and (b) constrained model.

Table 2. Predicted and observed widths for different vegetation types.

Vegetation type	Observed	Bank strength unconstrained model		Bank strength constrained model		
	W_{observed} (m)	$W_{\text{Predicted}}$ (m)	$W_{\text{Pred}}/W_{\text{obs}}$	ϕ' (degrees)	$W_{\text{Predicted}}$ (m)	$W_{\text{Pred}}/W^*_{\text{obs}}$
1	32.3	14.40	0.44	43.5	36.46	1.08
2	22.4	11.50	0.54	47.6	22.04	1.00
3	27.0	16.48	0.64	50.0	29.08	1.24
4	20.2	14.03	0.75	64.3	16.72	0.93

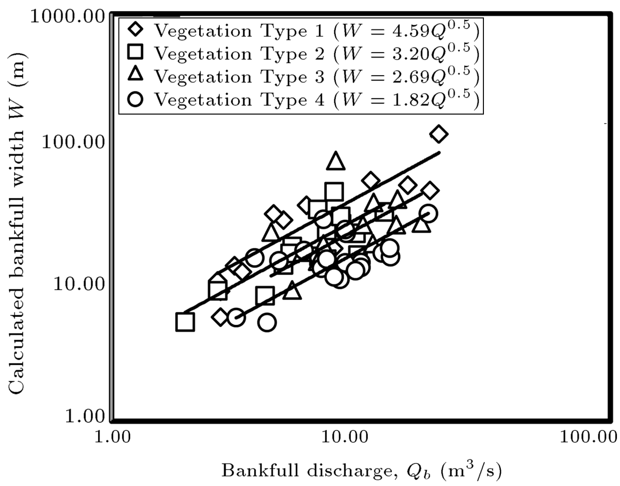

Figure 7. Relation between discharge and width for different types of vegetation.

researchers have suggested [29,31] that vegetation type does not cause variation in the power of width hydraulic geometry relationships. However, it may influence their coefficients. Hence, based on the conducted research studies, the width of hydraulic geometry is considered $W = aQ^{0.5}$. The model is applied with Manning's equation as resistance and Parker [24] as bed load equation to compute width for all types of vegetation. Therefore, values of 'a' are calibrated for each type by fitting $W = aQ^{0.5}$ to the data on log-log scale to obtain the following (Figure 7):

$$W = 4.59Q^{0.5}\text{m (Vegetation Type 1)}, \tag{34a}$$

$$W = 3.20Q^{0.5}\text{m (Vegetation Type 2)}, \tag{34b}$$

$$W = 2.69Q^{0.5}\text{m (Vegetation Type 3)}, \tag{34c}$$

$$W = 1.82Q^{0.5}\text{m (Vegetation Type 4)}. \tag{34d}$$

These equations indicate that for a given discharge, there is a decrease in channel width with increase in vegetation density. The observed and computed values of 'a' are compared for each vegetation type and relative errors are presented in Table 3. The results state a reasonable correspondence between computed and observed values of 'a'.

Table 3. Mean relative errors of 'a' values for $W = aQ^{0.5}$.

	Bank vegetation type			
	1	2	3	4
Mean relative error (%)	6.00	(3.90)*	(1.47)	(22.22)

*() indicates negative values (predicted values are less than observed values).

Case study 2. In this section, the data from the four river reaches of Iran (Khuzestan Province) are used [32]. The rivers are described as stable channels with movable gravel beds. The studied stations are located in the northern and eastern parts of Khuzestan, which are mountainous regions on the margin of the Zagros Mountains. The measured data including cross section, river channel slope, and Manning's roughness coefficient are made available at each hydrometric station by Khuzestan Water and Power Organization. The average size of bed particles and bankfull discharge were determined by Mahmoudi et al. [32]. It should be noted that bank angle (θ) cannot be found in the reference data and is therefore determined at each station using the AutoCAD software; cross section shapes for the two riverbanks and the mean values are used as the input data to the unconstrained model. In addition, because of the lack of bed load (Q_s) measurements in the data set, the constant slope state of the model is used for calibration. This section is meant to evaluate the efficiency of the presented model in working out river bank vegetation type by estimating ϕ' values. Therefore, the method presented in Section 3.2.1 for estimation of the angle of ϕ' is used by applying the developed model in this study and by combining the Manning and Parker equations [12,24], the calibrated values of ϕ' are obtained for the four studied river reaches. The results are presented in Table 4. Then, considering the estimated values of ϕ' in comparison with the range of the modified bank friction angles (Table 1) as well as the defined mean ϕ', the values with the minimum differences are used to estimate the riverbank vegetation. It should be noted

Table 4. Calibrated ϕ' values using Iranian data [32].

River	Station	ϕ' (°)	Predicted bank vegetation
Karoun	Sousan	61.5	4
Aab Shirin	Kheir Abad	59.8	3
Maroun	Cham Nezam	65.6	4
Zal	Pol-e-Zal	47.9	1

that the estimated ϕ' values are reasonable considering the location of studied river reaches and field surveys.

In the next sage, the model is used with regards to the Manning's flow resistance equation [12] combined with the Meyer-Peter and Muller [22], Parker [24], and modified Meyer-Peter and Muller by Huang [33] relations. In addition, the mean ϕ' values corresponding to different vegetation types according to Table 1 and other input data are considered with and without bank constraint. The model error (in percent) in estimation of the bankfull width and depth is presented in Table 5. The results clearly show better efficiency of the constrained model than the unconstrained model in estimation of the optimum channel dimensions for the studied river reach. The results also show better efficiency of the Meyer-Peter and Muller bed load function than others used for the studied reach.

4. Conclusion

The developed model in this study had great flexibility with regards to resistance and bed load equations. The model had a broad scope of applicability based on the available data.

Data analyses suggested that the predicted width values by MSTC and MSP under unconstrained condition were only valid in alluvial channels with highly resistant banks, so the model might not give correct results for erodible banks with sparse vegetation cover. Therefore, consideration of bank vegetation (constrained condition) might increase the accuracy of channel dimensions estimation to some extent, particularly in wide rivers with sparse vegetation cover.

Sensitivity analysis indicated that bed and surface widths could decrease by increasing bank vegetation or resistance while depth increased.

The model may also be applicable to the circumstances that ϕ' values require to be calibrated in assessing bank stability at a cross section of a river.

Nomenclature

Q	Discharge (m^3/s)
A	Cross-sectional area (m^2)
V	Mean velocity (m/s)
c_r	Coefficient
R	Hydraulic radius (m)
S	Longitudinal slope
D	Maximum channel depth (m)
x, y, α	Exponents
q_s	Bed load discharge per unit channel width
c_s	Coefficient
$\bar{\tau}_{\text{bed}}$	Mean bed shear stress (N/m^2)
τ_c	Critical shear stress (N/m^2)
m, j	Exponents
$\%SF_{\text{bank}}$	Percentage of the shear force acting on banks
P_{bed}	Bed perimeter
P_{bank}	Bank perimeter
$\bar{\tau}_{\text{bank}}$	Mean bank shear stress (N/m^2)
γ	Unit weight of water (N/m^3)
W	Channel surface width (m)
θ	Bank angle
z	Bank slope
τ^*_{cb}	Critical dimensionless shear stress for bank sediment
γ_s	Unit weight of sediment (N/m^3)
$D_{50\text{bank}}$	Bank material size
ϕ'	Bank friction angle
τ^*_c	Critical dimensionless shear stress
ϕ	Angle of repose
ζ	Non-dimensional channel shape factor

Table 5. Mean relative errors for different bed load equations.

Bed load equation	Unconstrained model		Constrained model	
	Bankfull width (%)	Bankfull depth (%)	Bankfull width (%)	Bankfull depth (%)
Meyer-Peter & Muller [22]	(25.57)*	23.65	3.12	(6.79)
MPM-H [33]	(29.13)	28.72	4.95	(7.62)
Parker [24]	(29.37)	29.57	6.98	(8.70)

*() indicates negative values (predicted values are less than observed values).

P	Channel perimeter (m)
Q_s	Bed load discharge
K	Variable
$D_{50\text{bed}}, D_{50}$	Bed material size

References

1. Bray, D.I. "Regime equations for gravel-bed rivers", In *Gravel-bed Rivers: Fluvial Processes, Engineering and Management*, R.D. Hey, J.C. Bathurst and C.R. Thorne, Eds., John Wiley and Sons, Chichester, pp. 517- 552 (1982b).
2. ASCE Task Committee on Hydraulics "Bank Mechanics and modeling of river width adjustment", *I: Processes and Mechanisms, J. Hydraul. Eng. ASCE*, **124**(9), pp. 881-902 (1998).
3. Leopold, L.B. and Langbein, W.B. "The concept of entropy in landscape evolution", *U.S. Geol. Survey. Prof. Paper* 500-A (1962).
4. Pickup, G. "Adjustment of stream channel shape to hydrologic regime". *Journal of Hydrology*, **30**, pp. 365-373 (1976).
5. Kirkby, M.J. "Maximum sediment efficiency as a criterion for alluvial channels", In *River Channel Changes*, K.J. Gregory, Ed., Wiley: Chichester, pp. 429-442 (1977).
6. Yang, C.T. "Potential energy and stream morphology", *Water Resources Research*, **7**, pp. 311-322 (1971a).
7. Yang, C.T., Song, C.C.S., and Woldenberg, M.J. "Hydraulic geometry and minimum rate of energy dissipation", *Water Resources Research*, **17**, pp. 1014-1018 (1981).
8. Song, C.S.S. and Yang, C.T. "Minimum stream power: theory", *J. Hydraul. Eng. ASCE*, **106**(9), pp. 1477-1488 (1980).
9. Huang, H.Q. and Nanson, G.C. "A stability criterion inherent in laws governing alluvial channel flow", *Earth Surface Processes and Landforms*, **27**(9), pp. 929-944 (2002).
10. Eaton, B.C. and Millar, R.G. "Optimal alluvial channel width under a bank stability constraint", *Geomorphology*, **62**, pp. 35-45 (2004).
11. Parker, G. "Surface-based bedload transport relation for gravel rivers", *Journal of Hydraulic Research*, **28**, pp. 417-436 (1990a).
12. Manning, R. "On the flow of water in open channels and pipes", *Transactions of the Institution of Civil Engineers of Ireland*, **20**, pp. 161-207 (1891).
13. Huang, H.Q., Deng, C., Nanson, G.C., Fan, B., Liu, X., Liu, T., and Ma, Y. "A test of equilibrium theory and a demonstration of its practical application for predicting the morphodynamics of the Yangtze River", *Earth Surface Processes and Landforms*, **39**, pp. 669-675 (2014).
14. Knighton, A.D., *Fluvial Forms and Processes*, Edward Arnold, London (1998).
15. Lane, E.W. "The design of stable channels", *Trans, ASCE*, **120**(2776), pp. 1234-1279 (1955b).
16. Millar, R.G. and Quick, M.C. "Stable width and depth of gravel-bed rivers with cohesive banks", *J. Hydr. Div. ASCE*, **124**(10), pp. 1005-1013 (1993).
17. Parker, G. "Hydraulic geometry of active gravel rivers", *Journal of the Hydraulics Division, ASCE*, **105**, pp. 1185-1201 (1979).
18. Lacey, G. "Flow in alluvial channels with sandy mobile beds", *Proceedings of the Institute of Civil Engineers*, London, **9**; and Discussion, **11**, pp. 145-164 (1958).
19. Brownlie, W.R. "Flow depth in sand-bed channels", *Journal of Hydraulic Engineering, ASCE*, **109**, pp. 959-990 (1983).
20. Einstein, H.A. "The bed-load function for sediment transportation in open channel flows", U.S. Department of Agriculture, Soil Conservation Service, Technical Bulletin, No. 1026 (1950).
21. Yang, C.T., *Sediment Transport: Theory and Practice*, McGraw-Hill (1996).
22. Meyer-Peter, E. and Muller, R. "Formulas for bed load transport", In *Proceedings of the 3rd Meeting of IAHR*, Stockholm, pp. 39-46 (1948).
23. Du Boys, P. "The Rhone and streams with movable beds", *Annales des Ponts et Chaussees*, Section 5, **18**, pp. 141-195 (1879).
24. Parker, G. "Hydraulic geometry of active gravel rivers", *Journal of the Hydraulics Division, ASCE*, **105**, pp. 1185-1201 (1979).
25. Flintham, T.P. and Carling, P.A. "The prediction of mean bed and wall boundary shear in uniform and compositely rough channels", In *River Regime*, John Wiley and Sons, White, W.P. Ed., pp. 267- 287 (1988).
26. Knight, D.W. "Boundary shear in smooth and rough channel", *Journal of the Hydraulics Division, ASCE*, **107**(7), pp. 839-851 (1981).
27. Knight, D.W., Demetriou, J.D., and Hamed, M.E. "Boundary shear in smooth rectangular channels", *Journal of the Hydraulic Engineering, ASCE*, **101**(4), pp. 405-422 (1984).
28. Henderson, F.M., *Open Channel Flow*, Macmillan Pub. Co., New York, p. 522 (1966).
29. Hey, R.D. and Thorne, C.R. "Stable channels with mobile gravel beds", *Journal of the Hydraulic Engineering, ASCE*, **112**(8), pp. 671- 689 (1986).
30. Darby, S.E. "Refined hydraulic geometry data for British Gravel-Bed Rivers", *Journal of Hydraulic Engineering*, **131**(1), pp. 60-64 (2005).

31. Andrews, E.D. "Bed material entrainment and the hydraulic geometry of gravel bed rivers in Colorado", *Bulletin of the Geological Society of America*, **95**, pp. 371-378 (1984).

32. Mahmoodi, M., Tabatabai, M.R.M., and Mousavi Nadoushani, S. "Role of extermal hypotheses in rivers hydraulic geometry relationships derivation", *Sharif Civil Engineering Journal*, **33.2**(2.1), pp. 49-60 (2017).

33. Huang, H.Q. "Reformulation of the bed load equation of Meyer-Peter and Müller in light of the linearity theory for alluvial channel flow", *Water Resources Research*, **46**(9), pp. 1-11 (2010).

Biographies

Mahsa Mahmoudi received her BSc in Civil Engineering as the top student in 2012 and her MSc in River Engineering from Shahid Beheshti University also as a top student in 2014. She is now a PhD candidate at University of Tehran. Mahsa Mahmoudi has always been a remarkably talented student with 3 published journal papers and 3 conference papers.

Mohammad Reza Majdzadeh Tabatabai was born in 1963 in Tehran, Iran. He graduated in Civil Engineering from King's College, University of London, in 1989 and did his MSc in Water Resources Engineering in Queens Mary and Westfield College of University of London in 1991. He also did his PhD in Modelling of Fluvial Processes in University of East Anglia in Britain and attended the Civil Engineering Department of University of British Columbia as a visiting professor in 2003-2004. He is currently assistant professor of River Engineering in Civil, Water and Environmental Engineering Department at Shahid Beheshti University.

Saeed Mousavi Nadoushani is a Faculty Member at Shahid Beheshti University. He is specialized in stochastic hydrology and flood management scheme with over 28 years of experience in academic activities, and has published quite a number of papers in international peer reviewed journals.